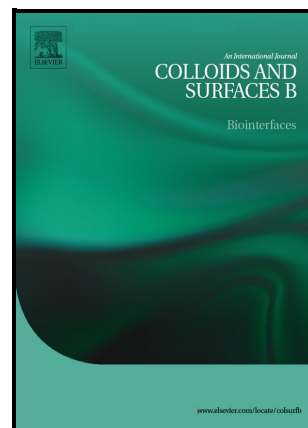# Journal Pre-proof

Graphene oxide reinforced hemostasis of gelatin sponge in noncompressible hemorrhage via synergistic effects

A Wenjing, Fanglin Du, Yinbo He, Bingxin Wu, Fang Liu, Yichun Liu, Weitao Zheng, Guofeng Li, Xing Wang

This is a PDF file of an article that has undergone enhancements after acceptance, such as the addition of a cover page and metadata, and formatting for readability, but it is not yet the definitive version of record. This version will undergo additional copyediting, typesetting and review before it is published in its final form, but we are providing this version to give early visibility of the article. Please note that, during the production process, errors may be discovered which could affect the content, and all legal disclaimers that apply to the journal pertain.

Graphene oxide reinforced hemostasis of gelatin sponge in noncompressible hemorrhage via synergistic effects

Wenjing A,[a] Fanglin Du,[a] Yinbo He,[a] Bingxin Wu,[a] Fang Liu,[b] Yichun Liu,[a] Weitao Zheng,[c] Guofeng Li,[a],* Xing Wang[a]

[a] *State Key Laboratory of Organic-Inorganic Composites, Beijing Laboratory of Biomedical Materials, Beijing University of Chemical Technology, Beijing, 100029, China*

[b] *Department of Oncology of Integrative Chinese and Western Medicine, China-Japan Friendship Hospital, Beijing, 100029, China*

[c] *Hubei Provincial Key Laboratory of Industrial Microbiology, Sino-German Biomedical Center, National "111" Center for Cellular Regulation and Molecular Pharmaceutics, Hubei University of Technology, Wuhan, 430068, Hubei Province, China*

Abstract

Effective hemostasis for noncompressible bleeding has been a key challenge because of the deep, narrow, and irregular wounds. Swellable gelatin is an available hemostatic material but is limited by weak mechanical strength and slow liquid absorption. Herein, the design of a gelatin and graphene oxide (GO) composite sponge (GP-GO) that possesses stable cross-linked networks and excellent absorbability, is reported. The GP-GOs are constructed via the thermal radical polymerization technique, using methacrylate gelatin (Gel-MA) and poly(ethylene glycol) diacrylate (PEGDA) as the crosslinker, while GO is uniformly fixed in the network via the curing reaction to further strengthen the stability. The optimized GP-GO$_5$ with GO addition (5 wt%) exhibits high porosity (> 90%), distinguished liquid absorption rate (106 ms), rapidly responsive swelling (422% expansion within 10 s), and stable mechanical properties. The addition of GO effectively reinforces coagulation stimulation of GP-GOs though the stimulation of platelets and the enrichment effect at the interface, significantly reducing the blood coagulation index (BCI) (< 20%). Hemostatic mechanism study indicated the liquid absorbability of GP-GOs is the critical foundation to trigger the subsequent physical expansion, blood cells enrichment, and coagulation stimulations. Besides, GP-GO$_5$ exhibits excellent biosafety assessed by hemolysis and cytotoxicity. Under the synergistic effects, the biocompatible GP-GO$_5$ showed excellent hemostatic properties in the hemostasis of severe bleeding and noncompressible wounds compared with a pure gelatin sponge (GP) and the commercial Celox^{TM}. This study demonstrated a promising candidate for practical application of noncompressible wound hemostasis.

Keywords: Gelatin; Graphene oxide; Hemostasis sponge; Noncompressible wound; Coagulation mechanism.

1 Introduction

Severe bleeding is life-threatening, which can occur both externally and internally, including extensive epidermal damage, arterial lacerations, and severe perforation bleeding [1]. Effective

intervention before hospitalization is of great significance for improving patient survival [2]. At present, a variety of hemostatic materials have been developed for emergency hemostasis, including gauze [3,4], bandage [5], hydrogel [6,7], powder [8], and so on . These hemostatic materials show good hemostasis for superficial trauma, but exhibit shortcomings in coping with noncompressible wounds caused by penetration and stab. Noncompressible wounds have faced the immediate challenge of being deep, narrow, and irregularly shaped [9,10]. The above hemostatic agents are either difficult to reach the bleeding site or are easily washed away by the blood, resulting in poor treatment outcomings. At the same time, the inconvenient packaging form and the poor coagulation performance also limit the treatment of noncompressible wounds with present hemostatic agents. There are urgently needed innovative hemostatic materials for noncompressible wound bleeding [11]. Compared with other hemostatic materials, the hemostatic sponge has the advantages of being compressible, easy to package, easy to fit, and staying on the bleeding site to form physical pressure [10,12]. The development of a hemostatic sponge capable of rapid hemostasis will be of considerable significance for the treatment of noncompressible wound bleeding.

Gelatin, a product of partial hydrolysis of collagen, is widely used in the field of biomedicine due to its unique advantages in terms of price, biocompatibility, biodegradability, and modifiability [13]. Gelatin has swelling properties. It can absorb 5 to 10 times the weight of water and swell. Previous studies on hemostatic sponges used gelatin as the main composition to generate physical compression through a higher swelling rate, thereby promoting hemostasis [14,15]. Gelatin is also able to aggregate and activate platelets and rapidly form stable blood clots [16]. However, the inherent low mechanical properties and slow liquid absorption rate of gelatin are detrimental to rapid hemostasis in noncompressible wounds [17]. Gelatin-based hemostatic sponges prepared by relying only on the non-covalent cross-linked networks usually show low mechanical properties, especially in the aqueous environment [18]. The non-covalent cross-linked networks are easily destroyed, which limit the application in hemostasis [19]. Additionally, the slow liquid absorption rate gives rise to the extended expansion equilibrium time of gelatin-based sponge, reducing the efficiency of wound filling and the final hemostasis [20,21]. Therefore, material compounding strategy is needed to improve its mechanical strength and water absorption rate, which is essential to enhance its hemostatic performance in noncompressible wounds.

Graphene oxide (GO) is a derivative of graphene that possesses abundant hydrophilic oxygen-containing functional groups, such as hydroxyl, epoxy, and carboxyl groups [22]. These hydrophilic end-groups accompanied by the hydrophobic backbone endow GO with amphiphilic properties. Due to these specific amphiphilic properties and unique two-dimensional sheet structure, GO exhibits ideal channels for water transportation, thereby improving the absorbability of materials [23,24]. Previously, we reported a series of GO-based hemostatic sponges, which confirmed their potential application as a wound dressing by rapidly liquid absorption [25,26]. In addition, the other study confirmed that upon contact with blood, GO induces a strong aggregation response in platelets. Its efficiency is comparable to that of thrombin [27]. Zhang et al. prepared a composite sponge of *N*-alkylated chitosan and GO. By exploring the optimal ratio, it was confirmed that the addition of a higher proportion of GO had more significant platelet activation and higher coagulation efficiency [28]. Besides, it was revealed that the excellent toughness and tensile properties of GO notably improve the mechanical strength of polysaccharide materials [29,30]. Therefore, it is believed that compounding GO would be able to ameliorate the physical

defects of the gelatin sponge and increase its coagulation stimulation, thereby developing into a novel hemostatic material for noncompressible wounds.

Here, we proposed a facile method for preparing a series of gelatin/GO composite sponges (GP-GOs) with different GO contents for hemostasis in noncompressible wounds. GP-GOs were constructed by covalent crosslinking of methacrylate gelatin (Gel-MA), poly(ethylene glycol) diacrylate (PEGDA), and GO using a thermal radical polymerization technique. GP-GOs were successfully prepared, and the liquid absorption properties, swelling properties, and mechanical strength were systematically characterized. The multiple coagulation mechanisms of the composite sponge were demonstrated using blood clotting testing, aggregation of platelets and erythrocytes, stimulation of platelets, and activation of the coagulation pathway. The rat femur injury model and rat liver puncture model were used to mimic acute trauma and noncompressible wound bleeding. They demonstrated the superior hemostatic effect of GP-GOs in vivo, which outperformed the commercial hemostat, Cleox[TM]. Therefore, these biocompatible GP-GOs showed good potential for hemostatic applications in noncompressible wounds.

2 Experiment

2.1 Materials

Gelatin was purchased from Solarbio Co. Gel-MA was prepared according to the report method [31]. Graphite (80 mesh) was purchased from Qingdao Jinrilai Co., Ltd., Shandong, China. The GO solution was prepared with the Hummers' method [32]. Celox[TM] was obtained from Medtrade Products Ltd. (Crewe, U.K.). Other reagents were obtained from Sinopharm Chemical Reagent Co., Ltd., and they were used as received without any further purification.

2.2 Preparation of GP-GO sponge

The GP-GOs were prepared by a thermal radical polymerization technique. Briefly, Gel-MA was dissolved in deionized water, and mixed with the crosslinked agent PEGDA. The mass ratio of Gel-MA: PEGDA was controlled at 1:1 (w/w). Then, GO solution (10 mg/mL) and the initiator APS were added and mixed thoroughly by a high-shear machine. GO accounted for 0, 1, 5, 10, and 20 wt% of the total solid mass, and the obtained GP-GOs were donated as GP, GP-GO$_1$, GP-GO$_5$, GP-GO$_{10}$, and GP-GO$_{20}$, respectively. The mass ratio of APS was controlled at 1:4 to the total solid content (w/w). The specific formula for the synthesis of GP-GOs were shown in Table S1. Finally, the mixed solution was put into a reaction vessel at 70 °C for 4 h, and then freeze-dried for 48 h to obtain a GP-GO composite sponge.

2.3 Characterizations

Gel-MA was characterized by 1H NMR, which was recorded on a Bruker AV III 400 spectrometer using D$_2$O (**Fig. S1**). A scanning electron microscope (SEM, Hitachi S-4700) was used to observe the microscopic morphology of the GP-GOs. Fourier transformed infrared spectroscopy (FTIR, PerkinElmer, Spectrum 100), element analysis (EA, Vario Elcube), and X-ray photoelectron spectra (XPS, KRATOS AXIS SUPRA) were used to investigate the chemical composition of the GP-GOs. Thermogravimetric analysis (TGA, Mettler Toledo TGA/DSC1/1100SF) was used to determine the graphene content composition of GP-GO5.

2.3 Porosity measurement

The porosity of GP-GOs was measured by previously reported methods [33]. Briefly, The pre-weighed sponge (W_0) was immersed in absolute ethanol, and the saturated weight (W_1) was recorded. The porosity calculation formula was as follows: Porosity = $(W_1 - W_0)/(\rho \times V)$. Among them, ρ is the density of absolute ethanol, and V is the volume of the sponge.

2.4 Liquid absorption measurement

The liquid absorbability of GP-GOs included the liquid absorption amount and the liquid absorption rate. The liquid absorption amount was measured by the weight loss method. A pre-weighed sponge (W_0) was immersed in water and recorded the saturated weight (W_1). The calculation formula of water absorption was as follows: Liquid absorption = $(W_1 - W_0)/W_0 \times 100\%$ [28]. The liquid absorption rate was recorded by high-speed cameras [25].

2.5 Expansion ratio measurement

The expansion ratio of the GP-GOs was calculated from the volume measured at a predetermined time [34]. A pre-measured volume of dry GP-GOs was soaked in water and swelled. At a predetermined time (within 120 s), the volume of the sponge was recorded. The calculation formula of the expansion ratio was as follows: Expansion ratio (%) = V_l/V_f, where V_l is the volume at the next moment, and V_f is the volume at the previous moment.

2.6 Rebound rate measurement

The rebound rate of GP-GOs was measured by the height measured by repeated compression of weights. A 100 g weight was pressed on the sample. Compress the height to 50% of the last height, and record the rebound height. Repeated the cycle 20 times, and the formula for calculating the rebound rate was as follows: Rebound rate (%) = $H_f/H_l \times 100\%$, where H_l is the height of the sponge before the last compression, and H_f is the height of the sponge after the rebound.

2.7 Hemostatic testing

2.7.1 In vitro blood clotting testing

The blood clotting index (BCI) of GP-GOs was measured by previously reported methods [35]. Anticoagulated whole blood was collected from SD rats. After the anticoagulated whole blood was incubated with GP-GOs for 5 min, the deionized water was added to make the blood cells swell and burst. The absorbance value of the sample solution at 540 nm was measured. The deionized water and PBS without added samples were used as negative and positive controls, respectively. The calculation formula of blood clotting index (BCI) was as follows: BCI (%) = $(Abs_{sample} - Abs_+) / (Abs_- - Abs_+) \times 100\%$.

2.7.2 In vivo hemostatic performance

This study strictly complied with the review opinions of the Laboratory Animal Welfare Ethics Committee of the China-Japan Friendship Hospital (No: zryhyy 21-21-10-01). All SD rats (250 ± 20 g, 7 weeks old, male) were purchased from Beijing Weitong Lihua Laboratory Animal Technology Co., Ltd. In this study, self-bleeding was used as the blank, and the commercial hemostatic material Cleox[TM] was used as the control. Before surgery, all rats were anesthetized

with 1.25 mL of 10% chloral hydrate (0.5 mL/100 g). The anesthetized SD rats were fixed on the operating table for experiments. After the experiment, the SD rats were immediately injected with air to the heart, and they died painlessly.

Femoral artery puncture: The inguinal artery was severed by a scalpel. The materials cover the arterial wound area, and were slightly peeled off every 10 s to determine the hemostatic time. The blood lose was determined by weighing the weight of the material before and after hemostasis [35].

Liver puncture: The surgical procedure was evaluated according to a reported method [36]. The experimental approach was as follows: The abdominal cavity was opened and exposed the liver. Then, the liver was clamped, and penetrated with a 7 mm punch. A waterproof surgical cloth was placed under the liver, and the filter paper was placed on the surgical fabric. For the experimental group, $GP-GO_5$ (7 mm, thickness 2 mm) was placed in the liver wound, and the bleeding time was recorded. The blood lose was determined by weighing the weight of the material and the filter papebefore and after hemostasis.

2.8 Hemostatic mechanism

Blood cells absorption: The blood cells absorbability of GP-GOs was evaluated according to a reported method [37]. Briefly, after the sponge was incubated with blood cells, the free blood cells on the surface of the sponges were washed with PBS. Deionized water was used to lyse the blood cells anchored in the sponges to get a hemoglobin solution. The blood cell adhesion capacity of the samples was measured based on the absorbance at a wavelength of 540 nm. The blood cell adsorption without the sample treatment was a blank control.

Platelet absorption: The platelet adhesion ability of the samples was measured by the lactate dehydrogenase (LDH) assay [38]. Lysates were measured by LDH assay kit (Solebold, China) to quantify the number of adherent platelets. The unadded sample group was used as a blank control to calculate the adsorption percentage.

SEM was used to observe microscopic morphological changes erythrocytes and platelets. A drop of blood cell dilution or whole blood was dropped onto the surface of the material, incubated at 37°C for 3 min, and washed with PBS 3 times to remove unabsorbed blood. After fixing with 2.5% glutaraldehyde solution at 4°C for 2 h, the samples were eluted with a series of gradient concentrations of ethanol and dried. The interfacial interactions of samples were observed by SEM after spraying gold.

Clinical standard coagulation tests: The prothrombin time (PT) and activated partial thromboplastin time (APTT) were tested with MC-2000 semiautomatic coagulation analyzer (TECO, Germany). The supernatant was collected from fresh blood by centrifugation to obtain platelet-poor plasma (PPP) [35]. The reagents were incubated with the samples for 30 min at 37 °C. PPP (50 μL) and 100 μL detection reagent (100 μL) were added to each measuring tube for testing. The pure PPP with no added sample was used as a control.

2.9 Biocompatibility

In vitro hemolysis test: The in vitro hemolysis test of GP-GOs was evaluated according to a reported method [39]. The anticoagulant 2 mL and PBS 8 mL were mixed to obtain an erythrocyte volume solution. The supernatant was removed by centrifuge 3 times. The washed red blood cells were diluted 10-fold to prepare erythrocyte suspension. The powdered sample (1 mg) was mixed

with 1 mL of erythrocyte suspension. Then they were incubated for 1 h at 37 °C, centrifuged at $2000 \times g$ for 15 min, and measured the absorbance of the supernatant at 540 nm. The negative control group consisted of 1 mL of red blood cell suspension, and 0.1 mL of red blood cells and 0.9 mL of deionized water were mixed as the positive control group. The calculation formula of hemolysis rate was as follows: Hemolysis rate (%) $= (Abs_{sample} - Abs_+) / (Abs_- - Abs_+) \times 100\%$.

Cytotoxicity test: The cytocompatibility of GP-GOs was investigated by the extraction solution method using rat fibroblast cells (L929) as a model. The sample powder was added to the medium to prepare a 5 mg/mL leaching solution and incubated for 24 h. After passing through the membrane, L929 cells were added to each well of a 96-well plate. After incubation for 24 h, the cells were subjected to an MTT assay. Finally, the absorbance value was measured at 570 nm. Biocompatibility results were calculated as the relative percentage of cell viability compared to untreated cells.

2.10 Statistical analysis

All data in this study were expressed as mean ± standard deviation. Each test was repeated at least 3 times. The two-tailed Student t-test was used to evaluate the selected samples, and the difference was considered significant when the statistical significance level was $p < 0.05$.

3 Results and discussion

3.1 Characterization of GP-GO

As **Fig. 1a** illustrated, the GP-GO hemostatic sponges were constructed via a thermal radical polymerization technique. The main cross-linked network was composed of Gel-MA and PEGDA. Gelatin is a hemostatic biological macromolecule with swelling properties, while PEGDA is a crosslinker to increase the crosslinking density. Besides, GO was added into the cross-linked network. It would be tightly firmed through the curing reaction between its epoxy groups and the amino groups of Gel-MA. GO strengths the GP-GO sponge, and importantly, it can activate platelets and trigger a coagulation cascade. To explore the effects of different contents of GO on physicochemical properties of the sponges, a series of GP-GOs were obtained by altering the content of GO (0 wt%, 1 wt%, 5 wt%, 10 wt%, and 20 wt%), namely GP, GP-GO$_1$, GP-GO$_5$, GP-GO$_{10}$, and GP-GO$_{20}$.

The morphologies of GP and GP-GOs were shown in **Fig. 1b**. After polymerization, GP and GP-GOs changed from a liquid state to a stable hydrogel state. After freeze-drying, the obtained GP was a tidy white sponge. With the addition of GO, GP-GOs were brown, and their surface gradually became rougher. Rough surfaces favored cell adhesion compared to smooth surfaces [17]. The SEM images clearly showed the pore structure of GP and GP-GOs (**Fig. 1b**). From the perspective of microstructure, GP had regular pore structures in both cross and rip sections. In the cross-section, the pore size of GP was approximately 100-200 μm. In the rip section, the regular interlayer structure could be observed obviously. The layer spacing was approximately 60-80 μm. For GP-GO$_1$, the connection between hole walls was discontinuous due to the GO sheets doping, and the interlayer structure was irregular. These changes were more distinct when the addition amount of GO was further increased to 5 and 10 wt%. The interlayer structure was loose and irregular, and the cross-section showed connected pores from several micrometers to several hundreds of micrometers. When the addition amount of GO was up to 20%, the obtained GP-GO$_{20}$

showed a completely irregular laceration structure both in the cross and rip sections. The results demonstrated that adding GO sheets decreased the number of cross-linkers. The GO sheets destroyed the compact linear structure of the sponge and drove the formation of a large number of micro-pores.

Accordingly, the specific surface area of GP-GOs would be increased in comparison with GP sponge. The porosity of GP-GOs increased with the increase of GO content (**Fig. 2a**). The porosity of GP-GO$_5$ was more than 90%, while that of GP was only $49.49 \pm 7.64\%$. These results were consistent with the SEM observation.
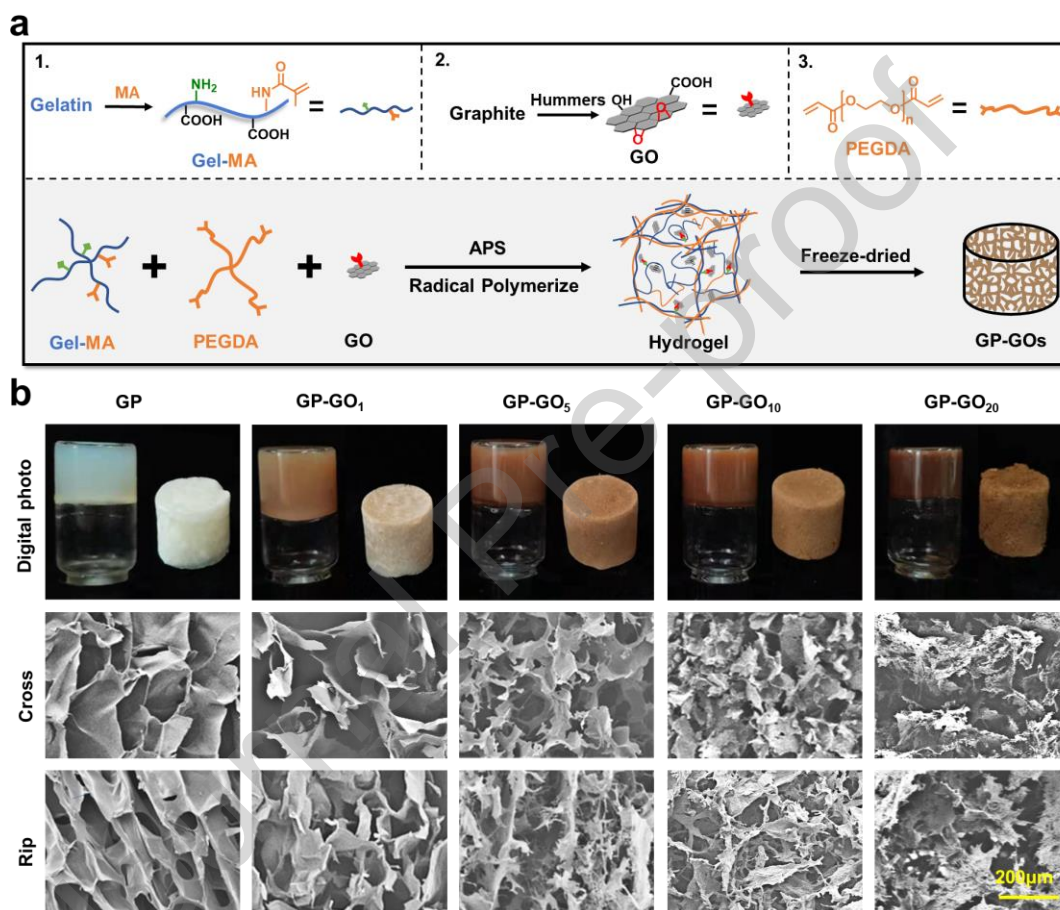

Fig. 1. Preparation and morphologies of GP and GP-GOs. (a) Schematic of the GP-GOs preparation. (b)The digital photo and SEM image of the GP and GP-GOs (scale = 200 μm)

The chemical structure of GP-GOs was investigated using FTIR (**Fig. 2b**) and XPS spectra (**Fig. 2c**). As shown in FTIR spectra, the characteristic peaks of GP-GOs appeared at 3330 cm^{-1} (C-OH stretching vibrations), 1734 cm^{-1} (C=O stretching vibrations), 1653 cm^{-1}, 543 cm^{-1} and 1248 cm^{-1} are respectively reclassified as amide I (peptide C=O stretching), amide II (N-H bending), and amide III (C-N stretching and N-H bending). Especially, the peak belonging to C=O stretching at 1653 cm^{-1} in GP-GOs spectra was obviously enhanced, suggesting that the curing reaction happened between the amino groups of Gel-MA and the epoxy groups of GO [40]. To prove this fact, the surface composition of GP and GP-GO$_5$ was further analyzed by XPS. The N 1s photoelectrons characteristic in GP and GP-GO$_5$ spectra were fitted by the XPS peak fit software (Fig. 2c). The N 1s peak could be characterized by contribution at 399.5, 400.1, and

401.6 eV, arising from the amine ($C\text{-}NH_2$), the amide (O=C-N-), and charged amine moieties (NH_3^+) [41]. It was clearly revealed that the amine groups in GP-GO$_5$ were significantly reduced. On the contrary, the amide groups were increased compared with those in GP, suggesting that GO was effectively immobilized in the structure by a curing reaction.

The composition of GP-GOs was investigated by elemental analysis and TGA tests. Elemental analysis showed the relative amount of each element (**Fig. 2d**). Out of all the raw materials, element N only existed in Gel-MA. That was, with the addition of GO, C/N would gradually increase. The results showed that the C/N mass ratio increased from 5.84 (GP, C 46.48; N 7.96) to 7.06 (GP-GO$_{20}$, C 47.47; N 6.72), confirming the successful construction of this series of GP-GOs with different GO additions [25]. In addition, represented by GP-GO$_5$, the decomposable and non-decomposable parts of the material were characterized by TGA (**Fig. S2**). The results showed that GP-GO$_5$ had a first-stage mass loss at about 200°C, mainly caused by GO reduction. The mass loss of the second step occurred at about 300°C, which might cause by GP decomposition. Thereby, the mass loss of each stage can be theoretically calculated that the GO content in GP-GO$_5$ was 5.08%, which was consistent with the actual additional amount.
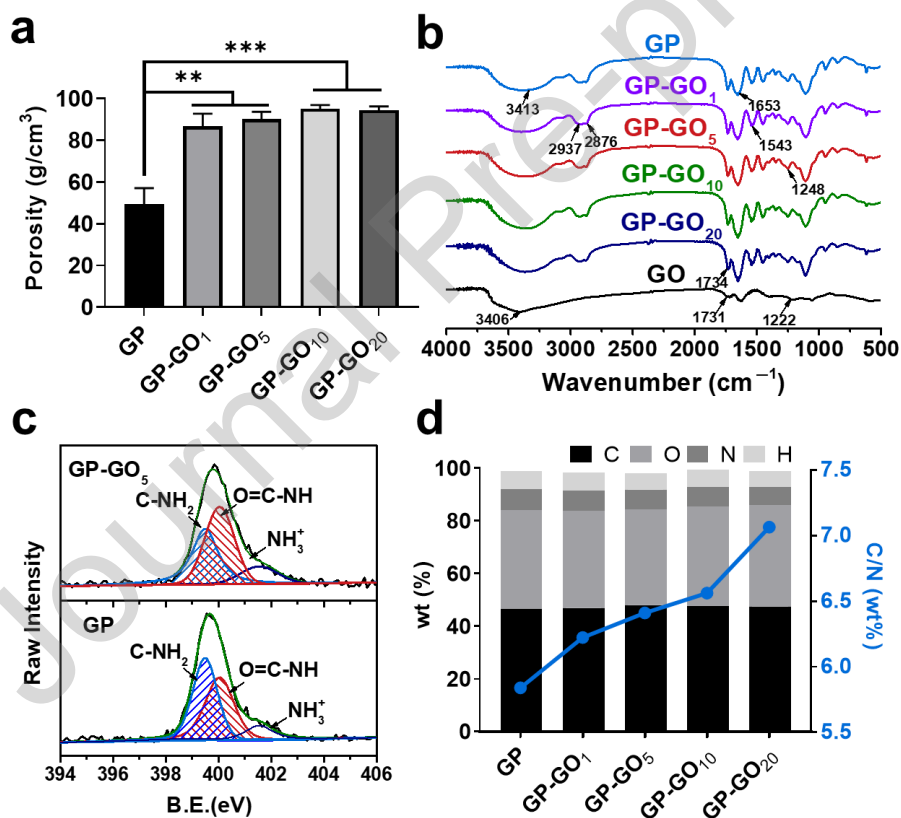

Fig. 2. Characterization of GP and GP-GOs. (a) The porosity of GP and GP-GOs. (b) FTIR spectra of GP and GP-GOs. (c) The results of fitting N 1s of XPS spectra of GP and GP-GO$_5$. (d) EA test and C/N of GP and GP-GOs. Data were presented as mean $\pm$ SD (n = 3); **p < 0.01, ***p < 0.001.

3.2 Absorption and mechanical properties

Based on the porous structure and specific surface area of GP-GOs, we speculated that

GP-GOs had good liquid absorption capacity. We subsequently evaluated the water absorption performance of GP-GOs from two levels. Firstly, the uncompressed sponges (1 cm × 0.36 cm^2) were placed in 3 mL of the water (methylene blue was added for observation) to assess the water absorption of the whole sponge. As shown in **Fig. 3a**, GP was a relatively hydrophobic sponge. It maintained the original morphology even though entirely exposed to the liquid. There was no apparent water absorption that occurred last for 5 s. Conversely, the GP-GOs exhibited a better liquid absorbability compared with GP. A significant improvement could be observed when the addition amount of GO was increased to 5 wt%. The fabricated GP-GO$_5$ absorbed water immediately at the moment of contact and rapidly expanded simultaneously. Finally, GP-GO$_5$ sucked up whole water within 3 s. GP-GO$_{10}$ showed a similar effect to GP-GO$_5$. When the amount of GO was added up to 20 wt%, the situation had changed. Although filled with liquid in the shortest time, the liquid absorption amount was significantly reduced, suggesting that adding too much GO would be detrimental to fluid absorption (**Fig. 3a**).

Subsequently, the liquid absorption rate of GP-GOs was characterized using a high-speed camera (**Fig. 3b**). When a droplet of water was dropped, it could stably stay on the surface of GP and was gradually absorbed not until 1200 ms. Significantly, GO could shorten the liquid absorption time of GP-GOs, and they were positively correlated with the addition amount of GO (**Fig. 3c**). Represented by GP-GO$_5$, a droplet of water could be absorbed entirely within 106 ms, 11 times faster than GP. This implied that GO was crucial for regulated the rapid liquid absorption behavior of GP-GO. For one thing, GO could alter the wettability of the gelatin sponge. The hydrophilic end-groups of GO effectively captured liquid. The subsequent rapid liquid transportation between GO nanosheets could be considered the frictionless transfer channel that accelerated the liquid internalization [23,24]. For another, appropriate but not excessive GO addition strengthened the mechanical strength of GP-GOs and created an abundant macro-porous structure that facilitated liquid storage. As **Fig. 3c** illustrated, adding 1 wt% of GO could increase the liquid absorbed amount of GP-GO$_1$, but more GO addition would gradually attenuate the liquid absorbed amount of GP-GOs. These results demonstrated that excessive GO addition worked as radical quencher that damaged the cross-linked network of GP-GOs, which resulted in pore collapse that attenuated liquid absorbability [42].

The expansion property of GP-GOs was evaluated (**Fig. 3d**). We first confirmed the expansion behavior of GP-GO in the incompressible state. GP showed 500 times expansion of its original volume after total liquid absorption. The expanded ratios of GP-GOs were negatively correlated with the additional amount of GO. The highest expansion capacity was around 400% for the GP-GO$_1$, followed by GP-GO$_5$ and GP-GP$_{10}$ with expansion ability of ~180% and 160%, respectively, and finally by the GP-GP$_{20}$ with an expansion ability of 114%. Nonetheless, the addition of GO significantly improved the expansion rate of GP-GOs. Within the first 10 s in contact with the liquid, the more GO added, the faster the expansion rate (inset in **Fig. 3d**). Considering the practical applications, GP-GOs would be more practical to stuff the wound in a compression situation. The GP-GOs, therefore, were compressed to 50% of their original volume to simulate the actual situation. GP-GOs exhibited a similar expansion rate to the uncompressed state. The GO content was positively correlated with the expansion rate (**Fig. S3**). The final expansion ratio of the water-swellable GP-GOs after compression was increased compared to the uncompressed state. Represented by GP-GO$_5$, GP-GO$_5$ can swell 422% within 10 s, which was benefit for blocking the bleeding point in such a short time. Meanwhile, GP-GO$_5$ was flexible and

was able to tailor into various shapes (**Fig. S4**), and the fast expansion rate of GP-GO$_5$ that compressed in a syringe could be also observed in a video (**Video S1**). Collectively, GP-GOs were compressible materials that would facilitate intimate contact with injured surfaces [43].

Subsequently, dynamic compressive strain tests were performed to characterize the mechanical strength of GP-GOs (**Fig. 3e**). In this assay, 50% compressive strain was employed onto GP-GOs by using a 100 g weight, and the resilience capacity of the compressed GP-GOs was observed without liquid absorption. Both GP and GP-GOs could rebound to more than 80% of their original height after 20 compression cycles, except for GP-GO$_{20}$. The resilience performance of GP-GO$_{20}$ disappeared after 5 cycles of compression, and some quality loss after 20 cycles of contraction. This could be attributed to the destruction of the irregular pore structure in GP-GO$_{20}$ after compression, which could not support the rebound of the sponges. Additionally, GP-GO$_5$ exhibited excellent compression flexibility and shape memory behavior. When GP-GO$_5$ was completely compressed in the dry state, it immediately recovered its original shape after immersing in water (**Fig. S5**). The shape recovery ability was maintained after repeated repetitions. Therefore, the addition of appropriate GO will enhance the stability of mechanical properties, which is of great significance for effectively resisting blood pressure shocks.
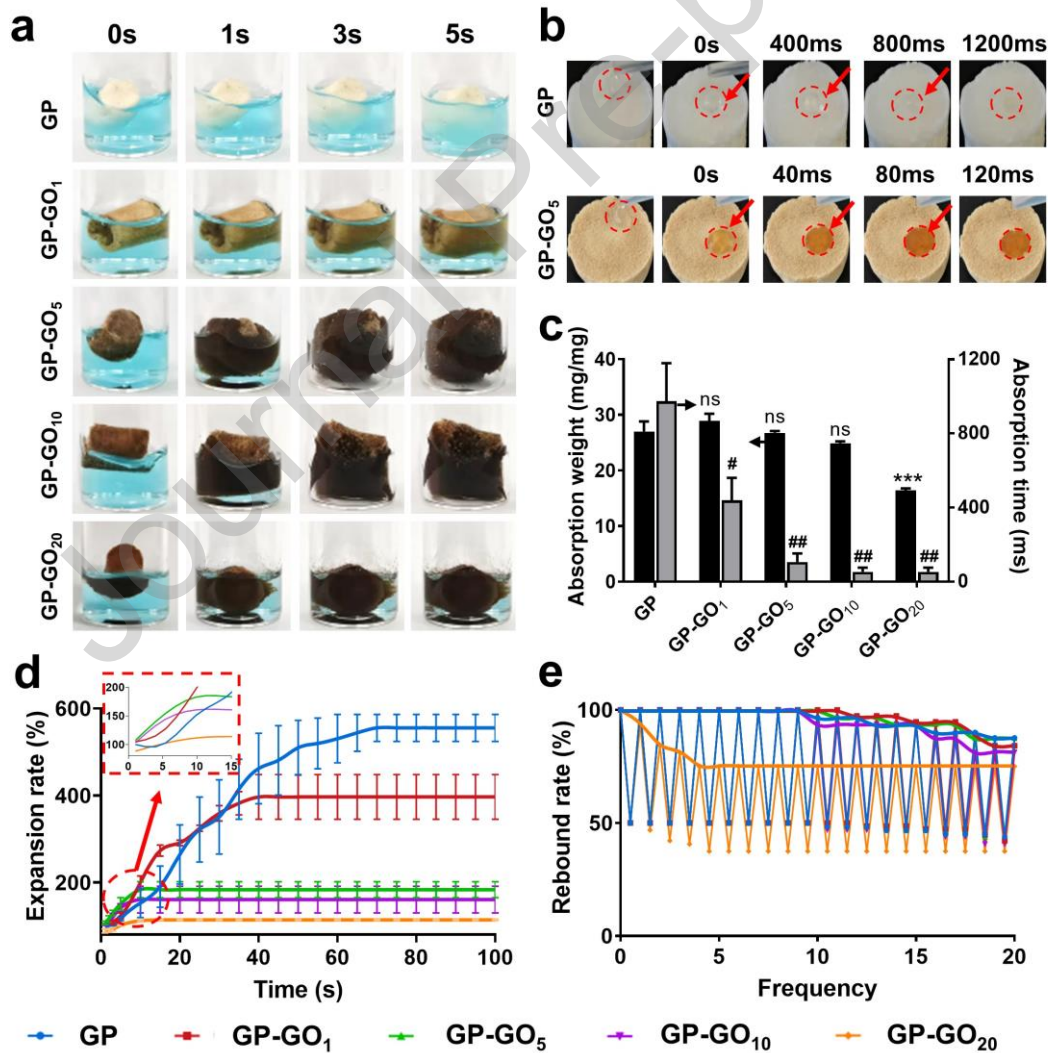

Fig. 3. Absorption and swell properties. (a) The morphological changes of GP and GP-GOs with

liquid absorption. (b) A drop in water absorption rate of GP and GP-GO$_5$. (c) The liquid absorption amount and rate of the sponges. (d) The expansion rate of the GP and GP-GOs. (e)The rebound rate of GP and GP-GOs. Data were presented as mean ± SD (n = 3); #p < 0.05, ##p < 0.01, ***p < 0.001.

3.3 Blood cell adsorption and activation

The absorption amount of red blood cells and platelet of GP-GOs were assessed (**Fig. 4a** and **4b**). After co-incubation for 30 min, the GP-GOs exhibited a significantly higher adhesion of platelets and red blood cells than GP. Their maximum absorption amounts were reached when using GP-GO$_5$, in which its absorption amount of platelet and red blood cells was 2.7 and 1.4 times higher than those of the GP. While further adding GO resulted in a negative output. These results could be attributed to the following aspects. The first and most important thing was that the stable and abundant pore structure and efficient fluid absorption capacity of GP-GOs played an essential role in capturing blood components [44]. Second, on the premise of rapid absorption, the main cross-linked network consisting of swellable gelatin captured liquid rapidly. GP-GOs expanded promptly, which played provided a larger specific surface area for the rapid adhesion and enrichment of blood cells and platelets. Thirdly, GO possessing abundant carboxyl groups activated platelets and induced their aggregation. When platelets were activated, ADP and thrombin A2 was released to accelerate the adhesion of more platelets [27]. To further demonstrate this viewpoint, the adhesive blood components on GP-GOs were intuitively observed by SEM (**Fig. 4c** and **4d**). GP-GO$_5$ was used as the representative and was co-incubated with whole blood in PBS. It could be clearly observed from the visual observation that many blood cells were gathered on the surface of GP-GO$_5$, and the blood cells have tightly adhered to the surface of the material. In turn, the control group GP had less adhesion to blood cells (**Fig. 4e**). At the same time, further enlarging the field of view, platelets were rarely observed in the GP group, and platelets in the activated state were even less so. The platelets on the surface of the intercepted GP-GO$_5$ were activated and tightly adhered to the material, which was accompanied by fibrous formation (red arrow in **Fig. 4f**). Apparently, GP-GO$_5$ promoted a large aggregation of platelets and red blood cells, which facilitated the rapid formation of blood scabs [45].
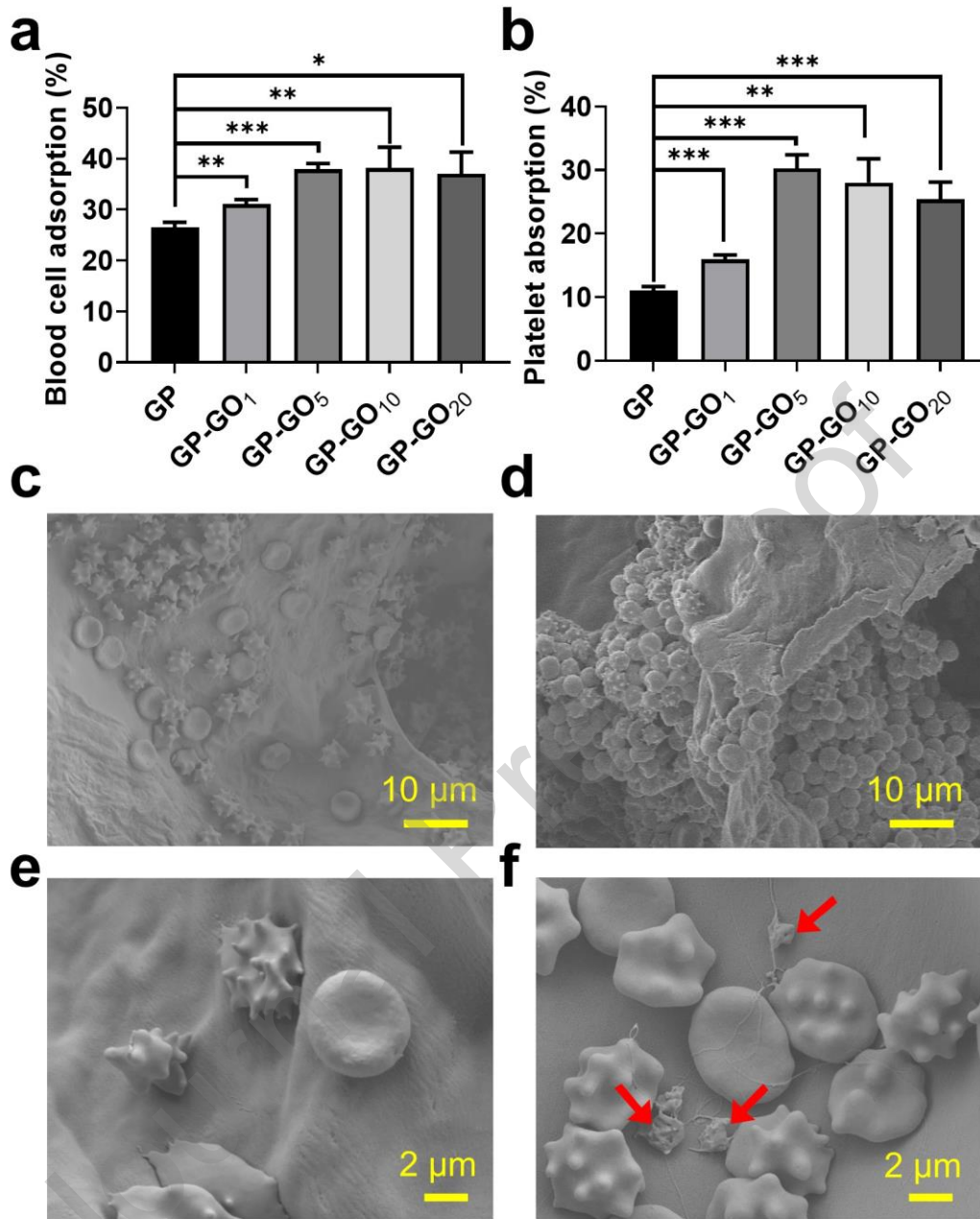
Fig. 4. Clotting properties. (a) The results of blood cell adsorption. (b) The results of platelet adsorption. (c) and (d) SEM of red blood cells in GP and GP-GO$_5$. (e) and (f) SEM of red blood cells and platelets in GP and GP-GO$_5$. Data were presented as mean ± SD (n = 3); *p < 0.05, **p < 0.01, ***p < 0.001.

3.4 In vitro coagulation behavior

The *in vitro* coagulation behaviors of the GP-GOs were then investigated. BCI is a commonly used method to evaluate the in vitro coagulation ability of hemostatic materials. **Fig. 5a** showed an optical photograph of the hemoglobin solution released from uncoagulated red blood cells. Compared with the control group GP, GP-GOs showed lighter color in vision. Statistical analysis showed that the BCI of all GP-GOs was lower than 17.5%, which was significantly lower than

that of GP (34.3 ± 2.8%) (**Fig. 5b**). The results of BCI showed that the GP-GO composite sponge significantly promoted blood coagulation. At the same time, we found that, under the premise of stable structure, the BCI value was positively correlated with porosity; *e.g.*, GP-GO$_{10}$ had the lowest BCI value (8.7 ± 2.6%), which was nearly 4 times lower than GP. Whereas for GP-GO$_{20}$, a slightly increased BCI value (14.1 ± 4.1%) was observed, confirming that the collapsed structure after absorbing water was not conducive to coagulation. Therefore, a synergistic effect of structural stability and clotting stimulation was essential for hemostasis.

To explore the coagulation mechanism of GP-GOs, the activation of GP-GOs on the coagulation cascade was studied. The coagulation cascade is involved in how blood clots are formed in the body. Through the combined pathway developed by the extrinsic pathway and the intrinsic pathway, each coagulation factor is activated. Finally, fibrin (factor Ia) is activated to seize the platelet to block and form a network, which promotes the formation of blood scabs [39,46]. **Fig. 5c** and **5d** showed the APTT and PT times of GP-GOs, GP, and the blank group, representing their intrinsic and extrinsic coagulation ability. Compared with the blank group (37.9 ± 1.6 s), GP could shorten the APTT time (31.0 ± 2.0 s). While introducing GO into GP, the obtained GP-GOs showed a shorter APTT time than GP because of the activation of coagulation factor XII by the negatively charged carboxyl functional group in GO. This implied that GP-GOs could trigger the intrinsic pathway of the coagulation cascade and accelerated coagulation [35]. For the extrinsic pathway, we found that the PT value of GP-GOs was not significantly different from that of the blank group. In other words, GP-GOs mainly activated endogenous pathways upon exposure to blood, thereby promoting thrombosis.
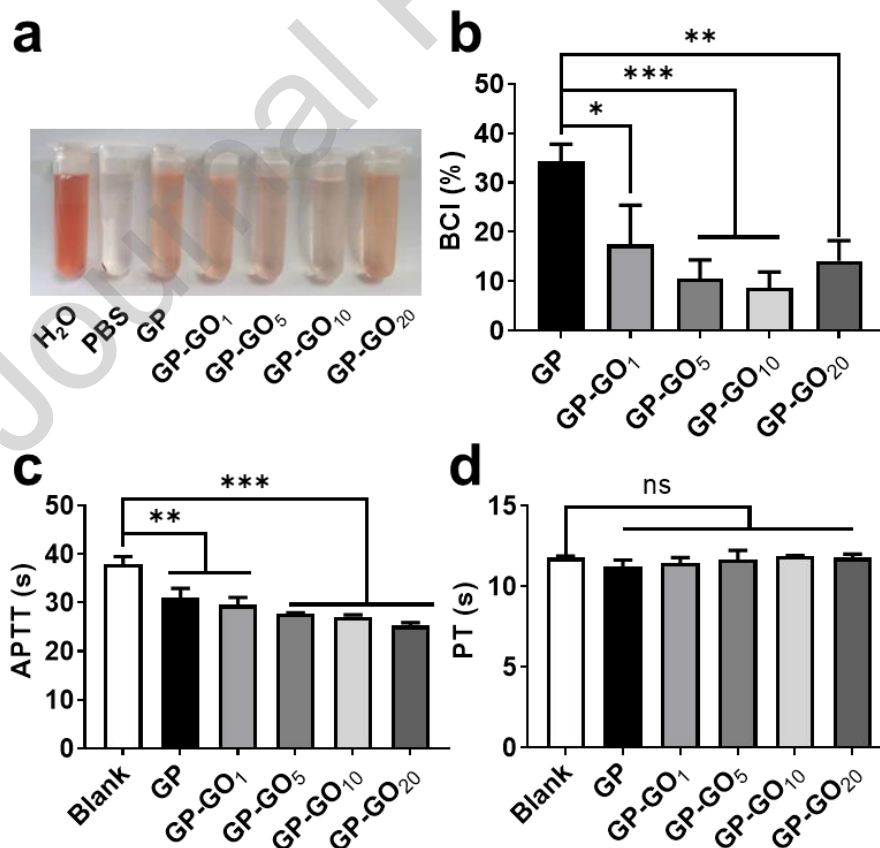

Fig. 5. In vitro hemostatic performance test. (a) BCI optical photograph. (b) The results of BCI

tests. (c) and (d) APTT and PT analysis of GP and GP-GOs. Data were presented as mean ± SD (n = 3); *p < 0.05, **p < 0.01, ***p < 0.001.

3.5 In vivo coagulation behavior

Based on careful consideration of liquid absorption performance, expansion performance, rapid resilience, and in vitro hemostasis performance evaluation, GP-GO$_5$ was finally selected as the final material for animal experiments. The rat arterial hemorrhage model and rat liver puncture model were used to evaluate the hemostatic performance of GP-GO$_5$ (**Fig. 6**). Celox™, one of the standard contents of the U.S. military first aid kit by the United States in 2010, was used as the control group [47,48].

The rat arterial hemorrhage model was first used (**Fig. 6a**). The rat femoral artery was severed entirely; GP-GO$_5$ was then used to cover the wound with constant pressure. When the wound was no longer bleeding after removing GP-GO$_5$, the times could be recorded as hemostatic time. Statistical results revealed that GP-GO$_5$ could stop bleeding within 77 ± 17 s, which was significantly shorter than GP and Celox^{TM} (117 ± 11 s and 101 ± 9 s) (**Fig. 6b**). Even more excitingly, the blood lost in the group of GP-GO$_5$ was only 0.96 ± 0.76 g, 62.0% and 64.1% less than those in the groups of GP and Celox^{TM}, respectively (**Fig. 6c**). Additionally, compared with GP, GP-GO$_5$ not only showed a significant hemostatic effect but also rapidly absorbed arterial hemorrhage without outflow during surgery. When hemostasis was completed, the material was opened, and there was prominent blood scab formation at the wound site. This implied that GP-GO$_5$ has excellent arterial an acute hemostatic ability.

Subsequently, rat liver puncture models mimic bleeding from noncompressible wounds (**Fig. 6d**). A hole with 7 mm diameter was made in the liver of the rat, and GP-GO$_5$ was inserted into the hole. GP-GO$_5$ quickly absorbed blood and exerted rapid resilience and expansion properties. The wound was sealed and stopped bleeding in the synergetic effects of physical compression and coagulation stimulations. The filter paper was used to collect the oozing blood (**Fig. 6e**). It was observed that apart from the group of GP-GO$_5$, all the other filter papers in the groups of the blank, GP and Celox™, showed significant blood oozing from the wound. GP-GO$_5$ expanded rapidly after bloodsucking, stopped bleeding within 36.0 ± 5.3 s (**Fig. 6f**), and the blood loss was only 0.20 ± 0.04 g (**Fig. 6g**). These two critical indicators in the group GP-GO$_5$ were the lowest among all the test groups. Besides, after hemostasis, GP-GO$_5$ was easily peeled off without secondary bleeding. For the commercially available hemostat Celox^{TM}, it was the powder that was highly adhesive to wounds after hemostasis and was not easily removed from wounds. These results confirmed that GP-GO$_5$ would be an excellent candidate for dealing with noncompressible wound bleeding.
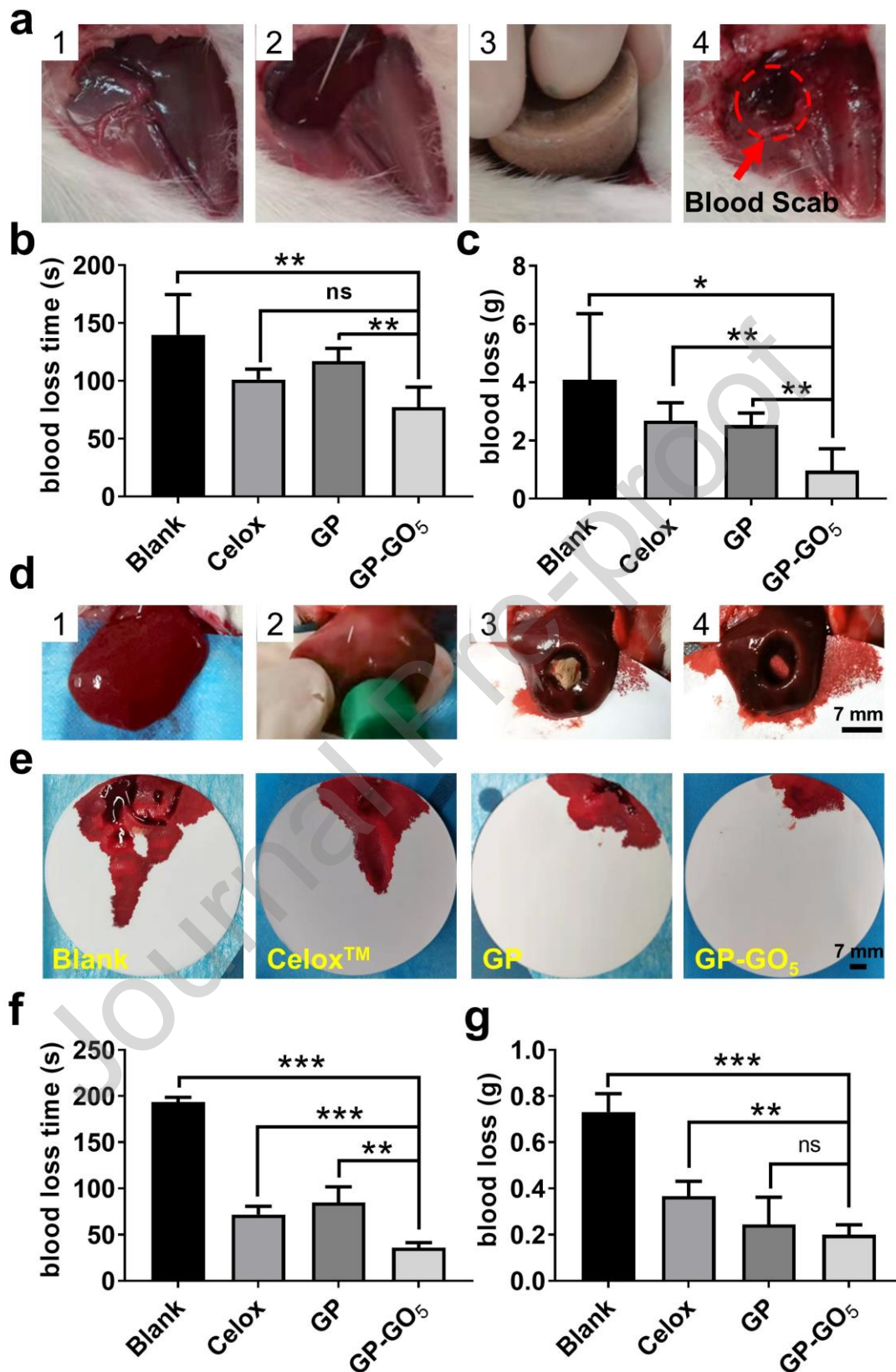
Fig. 6. Hemostasis in vivo. (a) The operational process of femoral artery hemostasis test (1: Expose the femoral artery, 2: Completely cut the femoral artery with a scalpel, 3: Sponge compression for hemostasis, 4: Complete hemostasis). (b) Hemostasis time of all samples in rat

femoral artery injury. (c) Blood loss of all samples in rat femoral artery injury. (d) Operation process of hepatic hemostatic test (1: Expose the liver, 2: Punch a penetrating liver defect with a diameter of 7mm, 3: Put a sponge into the defect to stop bleeding, 4: Stop bleeding completed). (e) The photo of blood stains on filter paper after hemostasis. (f) Hemostatic times and (g) blood loss of all samples in rat liver volume defect injury.Data were presented as mean ± SD (n = 3); *p < 0.05, **p < 0.01, ***p < 0.001.

The above studies demonstrated that $GP-GO_5$ possessed excellent hemostatic performance. It could be attributed to the synergistic effect of multi-mechanism of hemostasis, including physical interactions and coagulation stimulations (**Fig. 7**). As an essential foundation, GO addition enriched the pore structure and modulated the wettability of gelatin-based sponges, thereby endowed $GP-GO_5$ with astonishing liquid absorbability. When applied to an noncompressible wound, $GP-GO_5$ quickly absorbed the blood and triggered its rapid rebound and expansion. Within a short time, the wound was firmly extruded by $GP-GO_5$. In the presence of physical compression and accompanied by rapid liquid absorption, numerous platelets, and blood cells would be enriched at the interface between $GP-GO_5$ and the wound, forming an initial coagulation plug. Furtherly, plenty of platelets were activated and the intrinsic coagulation cascade were triggered by $GP-GO_5$, resulting in the formation of a stable fibrin network that accelerated coagulation.

Accordingly, the synergistic effect of multiple mechanisms plays a crucial role in the rapid hemostasis of noncompressible wounds. It was reported that hydrophilic hemostatic materials will lead to a large amount of blood loss because of their liquid absorbability, which is a negative effect on hemostasis [3,49]. Interestingly, $GP-GO_5$ possessed astonished liquid absorbability and also exhibited the best hemostatic performance, including shortest hemostatic time and lowest blood loss compared with Celox^{TM} and GP. The rapid liquid absorbability of $GP-GO_5$ was the critical foundation to trigger the subsequent physical rebound and expansion, blood cells and platelets enrichment, and coagulation stimulations [50]. Secondly, expansion capacity of GP-GOs, which was determined mainly by expansion ratio and speed, was essential for dealing with incompressible wounds [51]. Though GP possessed highest expansion ratio than GP-GOs, it exhibited an unsatisfactory hemostatic performance. As reported in the literature, the limited expansion speed affected subsequent hemostatic process, and the comprehensive properties, rather than expansion ratio, were essential for the hemostasis [52]. At the same time, structural stability is indispensable for the hemostatic effect of GP-GOs [53,54]. The pores collapse after liquid absorption would decrease the absorbability, weaken the enrichment of blood cells and platelets at the interface, which gave rise to the slow coagulation. Therefore, the multi-mechanisms synergy based on the rapid liquid absorption properties can effectively improve the hemostatic performance of the sponge.
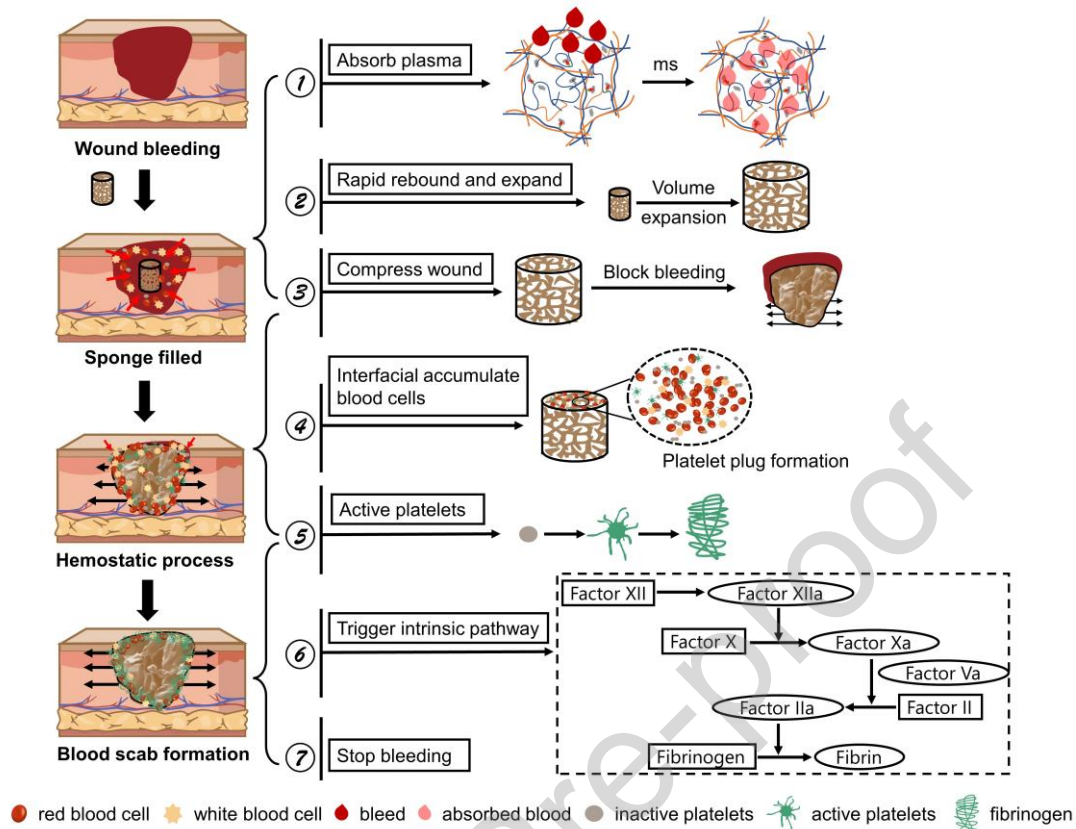
Fig. 7. Schematic illustration of the synergistic hemostasis mechanism for GP-GO.

3.6 Biocompatibility

In vitro hemolysis experiments were conducted to evaluate the blood compatibility of the raw materials Gel-MA, GO, GP, and GP-GO$_5$. As shown in **Fig. 8a**, the hemolysis rate of free GO was $12.8 \pm 0.4\%$, which was much higher than the hemolysis safety line of 5%. Conversely, the hemolysis rate of both Gel-MA, GP, and GP-GO$_5$ was less than 5%, indicating their good blood compatibility [55]. Additionally, cytotoxicity evaluation suggested that the cell survival rate in the GO group was reduced to a certain extent ($90.8 \pm 1.1\%$), which was slightly lower than that of blank cells but higher than the cell safety line of 80% (**Fig. 8b**). After fixing GO in the polymerization system by curing reaction, the cell survival rate of GP-GO$_5$ reached about 100%, indicating its cytocompatibility. Therefore, GP-GO$_5$ was a biocompatible hemostatic sponge.
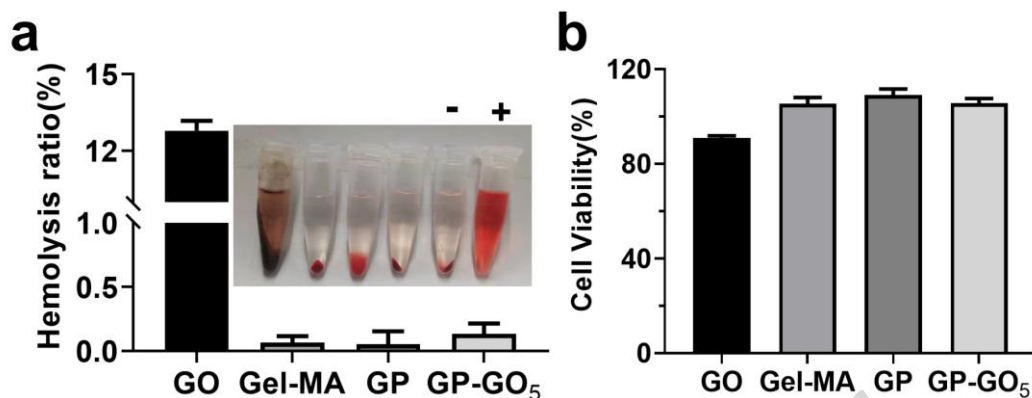
Fig. 8. Biocompatibility analysis. (a) Hemolysis ratios of GO, Gel-MA, GP, and GP-GO$_5$. (b) Cell viability of L929 cells. Data were presented as mean ± SD (n = 3).

4 Conclusion

We developed a series of gelatin/GO composite hemostatic sponges GP-GOs via radical polymerization. GO was uniformly distributed in the cross-linked network, which established numerous pore structures and provided effective liquid transport channels for GP-GOs. The obtained GP-GO with optimized GO addition amount (5 wt%) exhibited high porosity (> 90%), distinguished liquid absorption rate (106 ms), rapidly responsive swelling (422% expansion within 10 s), and stable mechanical properties. Meanwhile, in vitro coagulation experiments showed that the addition of GO significantly enhanced the coagulation stimulation of GP-GOs at the interface, and triggered the extrinsic cascade pathway to promote coagulation. Hemostatic mechanism studies revealed that the fluid absorption capacity of GP-GOs was the critical foundation to trigger the subsequent physical expansion, blood cells enrichment, and coagulation stimulations. Under these synergistic effects, GP-GOs exhibited excellent hemostatic properties, which were significantly better than the commercially available hemostatic agent Celox[TM] in both the rat femoral artery model and liver puncture model. Overall, our research demonstrated the importance of multi-mechanism synergistic hemostasis for incompressible wounds and provided a promising candidate for practical application of noncompressible wound hemostasis.

Declaration of Competing Interest

The authors declare no competing financial interest.

Acknowledgements

CRediT authorship contribution statement

X.W. and G.L. conceived the project. X.W., G.L., and W.A. designed the experiments. W.A.

performed experimental work and analyzed the data with help of F.D., Y.H., B.W., and Y.L.. In vivo coagulation assessments were performed with the help of F.L., F.D., and W. Z.. W.A. and G.L. drafted the manuscript. G.L., X.W., and F.D. edited the manuscript. All the authors discussed the results and commented on the manuscript.

References

[1]   P. Bouzat, G. Valdenaire, T. Gauss, J. Charbit, C. Arvieux, P. Balandraud, X. Bobbia, J.-S. David, J. Frandon, D. Garrigue, J.-A. Long, J. Pottecher, B. Prunet, B. Simonnet, K. Tazarourte, C. Trésallet, J. Vaux, D. Viglino, B. Villoing, L. Zieleskiewicz, C. Gil-Jardiné, E. Weiss, Early management of severe abdominal trauma, Anaesth. Crit. Care Pain Med. 39 (2020) 269–277.

[2]   R. Pfeifer, S. Halvachizadeh, S. Schick, K. Sprengel, K.O. Jensen, M. Teuben, L. Mica, V. Neuhaus, H.-C. Pape, are pre-hospital trauma deaths preventable? A systematic literature review, World J. Surg. 43 (2019) 2438–2446.

[3]   H. He, W. Zhou, J. Gao, F. Wang, S. Wang, Y. Fang, Y. Gao, W. Chen, W. Zhang, Y. Weng, Z. Wang, H. Liu, Efficient, biosafe and tissue adhesive hemostatic cotton gauze with controlled balance of hydrophilicity and hydrophobicity, Nat. Commun. 13 (2022) 552.

[4]   W. Zheng, C. Chen, X. Zhang, X. Wen, Y. Xiao, L. Li, Q. Xu, F. Fu, H. Diao, X. Liu, Layer-by-layer coating of carboxymethyl chitosan-gelatin-alginate on cotton gauze for hemostasis and wound healing, Surf. Coat. Technol. 406 (2021) 126644.

[5]   Y. Cui, Z. Huang, L. Lei, Q. Li, J. Jiang, Q. Zeng, A. Tang, H. Yang, Y. Zhang, Robust hemostatic bandages based on nanoclay electrospun membranes, Nat. Commun. 12 (2021) 5922.

[6]   L. Wang, M. Zhou, T. Xu, X. Zhang, Multifunctional hydrogel as wound dressing for intelligent wound monitoring, Chem. Eng. J. 433 (2022) 134625.

[7]   Q. Mao, O. Hoffmann, K. Yu, G. Lan, F. Dai, S. Shang, R. Xie, Self-contracting oxidized starch/gelatin hydrogel for noninvasive wound closure and wound healing, Mater. Des. 194 (2020) 108916.

[8]   X. Zhang, L. Jiang, X. Li, L. Zheng, R. Dang, X. Liu, X. Wang, L. Chen, Y.S. Zhang, J. Zhang, D. Yang, A bioinspired hemostatic powder derived from the skin secretion of andrias davidianus for rapid hemostasis and intraoral wound healing, Small. 18 (2022) 2101699.

[9]   Z.-Y. Zhang, H.-Y. Zhang, T. Talmy, Y. Guo, S.-R. Zhou, L.-Y. Zhang, Y. Li, Management of non-compressible torso hemorrhage: An update, Chin. J. Traumatol. 24 (2021) 125–131.

[10]   Q. Jiang, B. Luo, Z. Wu, B. Gu, C. Xu, X. Li, X. Wang, Corn stalk/AgNPs modified chitin composite hemostatic sponge with high absorbency, rapid shape recovery and promoting wound healing ability, Chem. Eng. J. 421 (2021) 129815.

[11]   Y. Huang, X. Zhao, C. Wang, J. Chen, Y. Liang, Z. Li, Y. Han, B. Guo, High-strength anti-bacterial composite cryogel for lethal noncompressible hemorrhage hemostasis: Synergistic physical hemostasis and chemical hemostasis, Chem. Eng. J. 427 (2022) 131977.

[12]   L. Yao, H. Gao, Z. Lin, Q. Dai, S. Zhu, S. Li, C. Liu, Q. Feng, Q. Li, G. Wang, X. Chen,

X. Cao, A shape memory and antibacterial cryogel with rapid hemostasis for noncompressible hemorrhage and wound healing, Chem. Eng. J. 428 (2022) 131005.

[13]   J. Alipal, N.A.S. Mohd Pu'ad, T.C. Lee, N.H.M. Nayan, N. Sahari, H. Basri, M.I. Idris, H.Z. Abdullah, A review of gelatin: Properties, sources, process, applications, and commercialisation, Mater. Today Proc. 42 (2021) 240–250.

[14]   O. Pinkas, M. Zilberman, Novel gelatin–alginate surgical sealants loaded with hemostatic agents, Int. J. Polym. Mater. Polym. Biomater. 66 (2017) 378–387.

[15]   J. Ranjbar, M. Koosha, H. Chi, A. Ghasemi, F. Zare, M.A. Abdollahifar, M. Darvishi, T. Li, Novel chitosan/gelatin/oxidized cellulose sponges as absorbable hemostatic agents, Cellulose. 28 (2021) 3663–3675.

[16]   X. Xie, D. Li, Y. Chen, Y. Shen, F. Yu, W. Wang, Z. Yuan, Y. Morsi, J. Wu, X. Mo, Conjugate electrospun 3D gelatin nanofiber sponge for rapid hemostasis, Adv. Healthc. Mater. 10 (2021) 2100918.

[17]   X. Wei, S. Ding, S. Liu, K. Yang, J. Cai, F. Li, C. Wang, S. Lin, F. Tian, Polysaccharides-modified chitosan as improved and rapid hemostasis foam sponges, Carbohydr. Polym. 264 (2021) 118028.

[18]   M. İnal, G. Mülazımoğlu, Production and characterization of bactericidal wound dressing material based on gelatin nanofiber, Int. J. Biol. Macromol. 137 (2019) 392–404.

[19]   L. Zheng, Q. Wang, Y.S. Zhang, H. Zhang, Y. Tang, Y. Zhang, W. Zhang, X. Zhang, A hemostatic sponge derived from skin secretion of Andrias davidianus and nanocellulose, Chem. Eng. J. 416 (2021) 129136.

[20]   G. Lan, B. Lu, T. Wang, L. Wang, J. Chen, K. Yu, J. Liu, F. Dai, D. Wu, Chitosan/gelatin composite sponge is an absorbable surgical hemostatic agent, Colloids Surf. B Biointerfaces. 136 (2015) 1026–1034.

[21]   X. Zhao, Y. Liang, B. Guo, Z. Yin, D. Zhu, Y. Han, Injectable dry cryogels with excellent blood-sucking expansion and blood clotting to cease hemorrhage for lethal deep-wounds, coagulopathy and tissue regeneration, Chem. Eng. J. 403 (2021) 126329.

[22]   G. Yang, Y. Wu, M. Liu, J. Liang, Q. Huang, J. Dou, Y. Wen, F. Deng, X. Zhang, Y. Wei, A novel method for the functionalization of graphene oxide with polyimidazole for highly efficient adsorptive removal of organic dyes, J. Mol. Liq. 339 (2021) 116794.

[23]   R.K. Joshi, P. Carbone, F.C. Wang, V.G. Kravets, Y. Su, I.V. Grigorieva, H.A. Wu, A.K. Geim, R.R. Nair, Precise and ultrafast molecular sieving through graphene oxide membranes, Science. 343 (2014) 752–754.

[24]   J. Zhang, K. Jia, Y. Huang, X. Liu, Q. Xu, W. Wang, R. Zhang, B. Liu, L. Zheng, H. Chen, P. Gao, S. Meng, L. Lin, H. Peng, Z. Liu, Intrinsic wettability in pristine graphene, Adv. Mater. 34 (2022) 2103620.

[25]   K. Quan, G. Li, D. Luan, Q. Yuan, L. Tao, X. Wang, Black hemostatic sponge based on facile prepared cross-linked graphene, Colloids Surf. B Biointerfaces. 132 (2015) 27–33.

[26]   B. Wu, F. Du, W. A, G. Li, X. Wang, Graphene-based hemostatic sponge, Chin. Chem. Lett. 33 (2022) 703–713.

[27]   S.K. Singh, M.K. Singh, M.K. Nayak, S. Kumari, S. Shrivastava, J.J.A. Grácio, D. Dash, Thrombus inducing property of atomically thin graphene oxide sheets, ACS Nano. 5 (2011) 4987–4996.

[28]   Y. Zhang, J. Guan, J. Wu, S. Ding, J. Yang, J. Zhang, A. Dong, L. Deng, N-alkylated

chitosan/graphene oxide porous sponge for rapid and effective hemostasis in emergency situations, Carbohydr. Polym. 219 (2019) 405–413.

[29] S. Guajardo, T. Figueroa, J. Borges, M. Meléndrez, K. Fernández, Comparative study of graphene oxide-gelatin aerogel synthesis: Chemical characterization, morphologies and functional properties, J. Inorg. Organomet. Polym. Mater. 31 (2021) 1517–1526.

[30] S. Mo, L. Peng, C. Yuan, C. Zhao, W. Tang, C. Ma, J. Shen, W. Yang, Y. Yu, Y. Min, A. J. Epstein, Enhanced properties of poly(vinyl alcohol) composite films with functionalized graphene, RSC Adv. 5 (2015) 97738–97745.

[31] Z. Luo, W. Sun, J. Fang, K. Lee, S. Li, Z. Gu, M.R. Dokmeci, A. Khademhosseini, Biodegradable gelatin methacryloyl microneedles for transdermal drug delivery, Adv. Healthc. Mater. 8 (2019) 1801054.

[32] H. Yu, B. Zhang, C. Bulin, R. Li, R. Xing, High-efficient synthesis of graphene oxide based on improved hummers method, Sci. Rep. 6 (2016) 36143.

[33] K. Quan, G. Li, L. Tao, Q. Xie, Q. Yuan, X. Wang, Diaminopropionic acid reinforced graphene sponge and its use for hemostasis, ACS Appl. Mater. Interfaces. 8 (2016) 7666–7673.

[34] P. Li, L. Cao, F. Sang, B. Zhang, Z. Meng, L. Pan, J. Hao, X. Yang, Z. Ma, C. Shi, Polyvinyl alcohol/sodium alginate composite sponge with 3D ordered/disordered porous structure for rapidly controlling noncompressible hemorrhage, Mater. Sci. Eng. C. (2022) 112698.

[35] Y. Liang, C. Xu, F. Liu, S. Du, G. Li, X. Wang, Eliminating heat injury of zeolite in hemostasis via thermal conductivity of graphene sponge, ACS Appl. Mater. Interfaces. 11 (2019) 23848–23857.

[36] X. Du, L. Wu, H. Yan, Z. Jiang, S. Li, W. Li, Y. Bai, H. Wang, Z. Cheng, D. Kong, L. Wang, M. Zhu, Microchannelled alkylated chitosan sponge to treat noncompressible hemorrhages and facilitate wound healing, Nat. Commun. 12 (2021) 4733.

[37] C. Wang, H. Niu, X. Ma, H. Hong, Y. Yuan, C. Liu, Bioinspired, injectable, quaternized hydroxyethyl cellulose composite hydrogel coordinated by mesocellular silica foam for rapid, noncompressible hemostasis and wound healing, ACS Appl. Mater. Interfaces. 11 (2019) 34595–34608.

[38] Z. Chen, L. Han, C. Liu, Y. Du, X. Hu, G. Du, C. Shan, K. Yang, C. Wang, M. Li, F. Li, F. Tian, Correction: A rapid hemostatic sponge based on large, mesoporous silica nanoparticles and *N* -alkylated chitosan, Nanoscale. 12 (2020) 14926–14926.

[39] G. Li, K. Quan, C. Xu, B. Deng, X. Wang, Synergy in thrombin-graphene sponge for improved hemostatic efficacy and facile utilization, Colloids Surf. B Biointerfaces. 161 (2018) 27–34.

[40] Y. Cheng, S. Lu, Z. Hu, B. Zhang, S. Li, P. Hong, Marine collagen peptide grafted carboxymethyl chitosan: Optimization preparation and coagulation evaluation, Int. J. Biol. Macromol. 164 (2020) 3953–3964.

[41] M. Abolhassani, C.S. Griggs, L.A. Gurtowski, J.A. Mattei-Sosa, M. Nevins, V.F. Medina, T.A. Morgan, L.F. Greenlee, Scalable chitosan-graphene oxide membranes: The effect of go size on properties and cross-flow filtration performance, ACS Omega. 2 (2017) 8751–8759.

[42] C. Zhang, S. Chen, P.J.J. Alvarez, W. Chen, Reduced graphene oxide enhances

horseradish peroxidase stability by serving as radical scavenger and redox mediator, Carbon. 94 (2015) 531–538.

[43]   Z. Li, B. Li, X. Li, Z. Lin, L. Chen, H. Chen, Y. Jin, T. Zhang, H. Xia, Y. Lu, Y. Zhang, Ultrafast in-situ forming halloysite nanotube-doped chitosan/oxidized dextran hydrogels for hemostasis and wound repair, Carbohydr. Polym. 267 (2021) 118155.

[44]   Y. Wan, J. Han, F. Cheng, X. Wang, H. Wang, Q. Song, W. He, Green preparation of hierarchically structured hemostatic epoxy-amine sponge, Chem. Eng. J. 397 (2020)

[45]   R.C. Reimers, S.P. Sutera, J.H. Joist, Potentiation by red blood cells of shear-induced platelet aggregation: relative importance of chemical and physical mechanisms, Blood. 64 (1984) 1200–1206.

[46]   S.P. Bajaj, J.H. Joist, New insights into how blood clots: Implications for the use of aptt and pt as coagulation screening tests and in monitoring of anticoagulant therapy, Semin. Thromb. Hemost. 25 (1999) 407–418.

[47]   B.L. Bennett, L. Littlejohn, Review of new topical hemostatic dressings for combat casualty care, Mil. Med. 179 (2014) 497–514.

[48]   M. Pozza, R. Millner, Celox (chitosan) for haemostasis in massive traumatic bleeding: Experience in Afghanistan, Eur. J. Emerg. Med. Off. J. Eur. Soc. Emerg. Med. (2011).

[49]   Z. Li, A. Milionis, Y. Zheng, M. Yee, L. Codispoti, F. Tan, D. Poulikakos, C.H. Yap, Superhydrophobic hemostatic nanofiber composites for fast clotting and minimal adhesion, Nat. Commun. 10 (2019) 5562.

[50]   O. Goncharuk, O. Korotych, Yu. Samchenko, L. Kernosenko, A. Kravchenko, L. Shtanova, O. Tsymbalyuk, T. Poltoratska, N. Pasmurtseva, I. Mamyshev, E. Pakhlov, O. Siryk, Hemostatic dressings based on poly(vinyl formal) sponges, Mater. Sci. Eng. C. 129 (2021)

[51]   Y. Wang, Y. Zhao, L. Qiao, F. Zou, Y. Xie, Y. Zheng, Y. Chao, Y. Yang, W. He, S. Yang, Cellulose fibers-reinforced self-expanding porous composite with multiple hemostatic efficacy and shape adaptability for uncontrollable massive hemorrhage treatment, Bioact. Mater. 6 (2021) 2089–2104.

[52]   X. Yang, M. Chen, P. Li, Z. Ji, M. Wang, Y. Feng, C. Shi, Fabricating poly(vinyl alcohol)/gelatin composite sponges with high absorbency and water-triggered expansion for noncompressible hemorrhage and wound healing, J. Mater. Chem. B. 9 (2021) 1568–1582.

[53]   X. Fan, Y. Li, N. Li, G. Wan, M.A. Ali, K. Tang, Rapid hemostatic chitosan/cellulose composite sponge by alkali/urea method for massive haemorrhage, Int. J. Biol. Macromol. 164 (2020) 2769–2778.

[54]   L.K. Jang, G.K. Fletcher, M.B.B. Monroe, D.J. Maitland, Biodegradable shape memory polymer foams with appropriate thermal properties for hemostatic applications, J. Biomed. Mater. Res. A. 108 (2020) 1281–1294.

[55]   T. Yan, F. Cheng, X. Wei, Y. Huang, J. He, Biodegradable collagen sponge reinforced with chitosan/calcium pyrophosphate nanoflowers for rapid hemostasis, Carbohydr. Polym. 170 (2017) 271–280.

CRediT authorship contribution statement

G.L. and X.W. conceived the project. G.L., X.W., and W.A. designed the experiments. W.A. performed experimental work and analyzed the data with help of F.D., Y.H., B.W., and Y.L.. In vivo coagulation assessments were performed with the help of F.L., F.D., and W. Z.. W.A. and G.L. drafted the manuscript. G.L., X.W., and F.D. edited the manuscript. All the authors discussed the results and commented on the manuscript.

Declaration of Competing Interest

The authors declare that they have no known competing financial interests or personal relationships that could have appeared to influence the work reported in this paper.

Graphical abstract
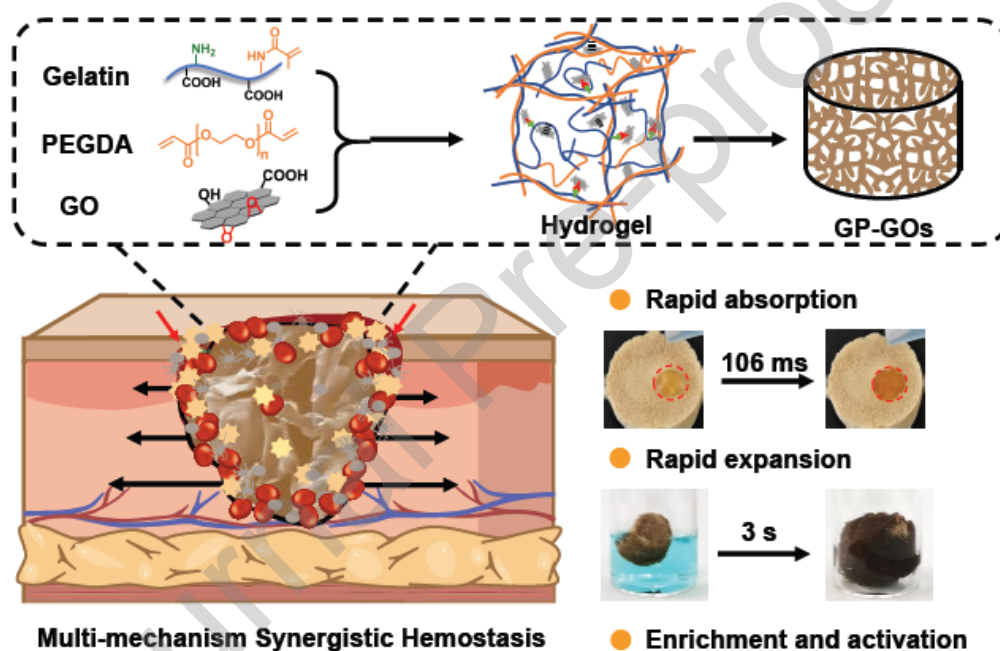
Highlights

- A series of GP-GOs with stable covalently cross-linked networks are prepared.
- GO efficiently reinforces liquid absorption and coagulation stimulation of GP-GO.
- Absorbability of GP-GO is critical for its multi-mechanism synergistic hemostasis.
- Hemostasis of GP-GO for noncompressible wound significantly outperforms the hemostat.